Ultrafast Science
A SCIENCE PARTNER JOURNAL

RESEARCH ARTICLE

Compressed Sensing of Field-Resolved Molecular Fingerprints Beyond the Nyquist Frequency

Kilian Scheffter[1,2], Jonathan Will[1,2], Claudius Riek[3], Herve Jousselin[4], Sébastien Coudreau[4], Nicolas Forget[4], and Hanieh Fattahi[1,2*]

[1]Max Planck Institute for the Science of Light, Staudtstr. 2, 91058 Erlangen, Germany. [2]Friedrich-Alexander University Erlangen-Nürnberg, Staudtrstr. 7, 91058 Erlangen, Germany. [3]Zurich Instruments Germany, Mühldorfstraße 15, 81671 Munich, Germany. [4]Fastlite, rue des Cistes 165, 06600 Antibes, France.

*Address correspondence to: hanieh.fattahi@mpl.mpg.de

Citation: Scheffter K, Will J, Riek C, Jousselin H, Coudreau S, Forget N, Fattahi H. Compressed Sensing of Field-Resolved Molecular Fingerprints Beyond the Nyquist Frequency. *Ultrafast Sci.* 2024;4:Article 0062. https://doi.org/10.34133/ultrafastscience.0062

Submitted 12 December 2023
Accepted 1 April 2024
Published 9 May 2024

Ultrashort time-domain spectroscopy and field-resolved spectroscopy of molecular fingerprints are gold standards for detecting samples' constituents and internal dynamics. However, they are hindered by the Nyquist criterion, leading to prolonged data acquisition, processing times, and sizable data volumes. In this work, we present the first experimental demonstration of compressed sensing on field-resolved molecular fingerprinting by employing random scanning. Our measurements enable pinpointing the primary absorption peaks of atmospheric water vapor in response to terahertz light transients while sampling beyond the Nyquist limit. By drastically undersampling the electric field of the molecular response at a Nyquist frequency of 0.8 THz, we could successfully identify water absorption peaks up to 2.5 THz with a mean squared error of 12×10^{-4}. To our knowledge, this is the first experimental demonstration of time-domain compressed sensing, paving the path toward real-time field-resolved fingerprinting and acceleration of advanced spectroscopic techniques.

Introduction

Detailed description of matter's constituent and internal dynamics is mirrored in its transient response to an external field. Resolving and monitoring the encoded information in the electric field of the ultrashort excitation field or in the time-dependent changes of the optical properties of the sample provides deep understanding and insights of matter [1,2]. The availability of few-cycle pulses has not only advanced various spectroscopic methods such as pump–probe spectroscopy and Fourier transform spectroscopy but has also led to the emergence of innovative techniques such as dual-comb spectroscopy and field-resolved spectroscopy [3–14].

Employing ultrashort pulses offers 2 distinct advantages for spectroscopic applications (Fig. 1). Firstly, their broad spectral bandwidth enables simultaneous data acquisition of the sample, eliminating the need for repeated measurements or laser tuning. With high-bandwidth acquisition, prior knowledge of the sample is not required, as all available information can be extracted from the measurement during postprocessing. Secondly, their extreme temporal confinement allows for temporal gating of the sample's response from the excitation pulses. This response, enriched with comprehensive spectroscopic information, lasts from tens of femtoseconds to nanoseconds and is commonly probed by a shorter pulse at various time intervals. When combined with additional temporal or spatial dimensions, such as multidimensional coherent spectroscopy [15], 4-dimensional imaging [16], and hyperspectral imaging [17], ultrashort spectroscopic techniques render the quantitative, multivariate characterization of the sample under scrutiny and facilitate the identification of unknown constituents. However, real-time measurements are prevented due to the need to record the high-bandwidth spectrum at each pixel image and time delay, which results in a prohibitively long acquisition time to attain sufficient signal-to-noise ratio. The measurement speed is limited to (a) the required number of sample points dictated by the Nyquist–Shannon criteria, (b) the speed of spatio-temporal scanning, and (c) the transportation and storage speed of the measured data. Although using short, high-bandwidth excitation pulses offers substantial benefits, such as simultaneous data acquisition, the sample response is often a linear combination of K basis vectors leading to a K-sparse frequency domain. Applying algorithms to the acquisition process is necessary to minimize data redundancy and obtain the desired spectral content with the minimum required data.

According to the Nyquist–Shannon sampling theorem, for a given sampling rate, the maximum resolvable frequency of a signal, called Nyquist frequency, is defined as half the sampling rate ($f_{\mathrm{Nyquist}} = f_{\mathrm{samp}}/2$). This criterion imposes a boundary for the minimum required data points necessary for successfully sampling a signal. Compressed sensing can circumvent this fundamental barrier by exploiting sparsity and incoherence of the signal, enabling the recovery of the original signal from fewer samples or measurements while preserving its quality [18–23].

The prior knowledge of a signal's sparsity enables the formulation of an optimization problem that allows for the reconstruction of the signal using a reduced number of sampling points below the Nyquist–Shannon criteria. The sparsity of the measured spectroscopic information of various materials has been discussed by analytical treatment in oversampled measurements [24–28] or analytical compression before storage or transmission [29,30]. However, the requirement for incoherence and random sampling has hindered the experimental demonstration of real-time, time-domain sparse sampling. This work demonstrates real-time, field-resolved compressed sensing of water vapor molecules beyond the Nyquist criteria. The reconstruction of the absorption spectrum of water vapor sets clear boundaries on the required sample sparsity for the effectiveness of compressed sensing, as the absorption spectrum includes both high-cross-section peaks and low-amplitude adjacent peaks. The real-time measurement in our approach is enabled by random sampling, using a rapidly scanning delay line and a fast reconstruction algorithm for real-time data analysis.

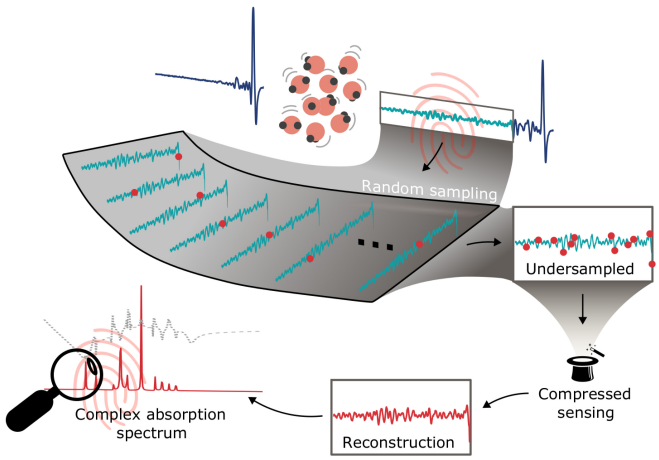

Fig. 1. Visual summary of compressed sensing of field-resolved molecular fingerprints.

Methods

Experimental setup

Figure 2A shows the experimental setup for terahertz (THz) field-resolved compressed sensing. The laser delivered 54-fs pulses centered at 810 nm with 2.1-mJ energy at 1-kHz repetition rate. In the setup, the diameter of the beam was first reduced

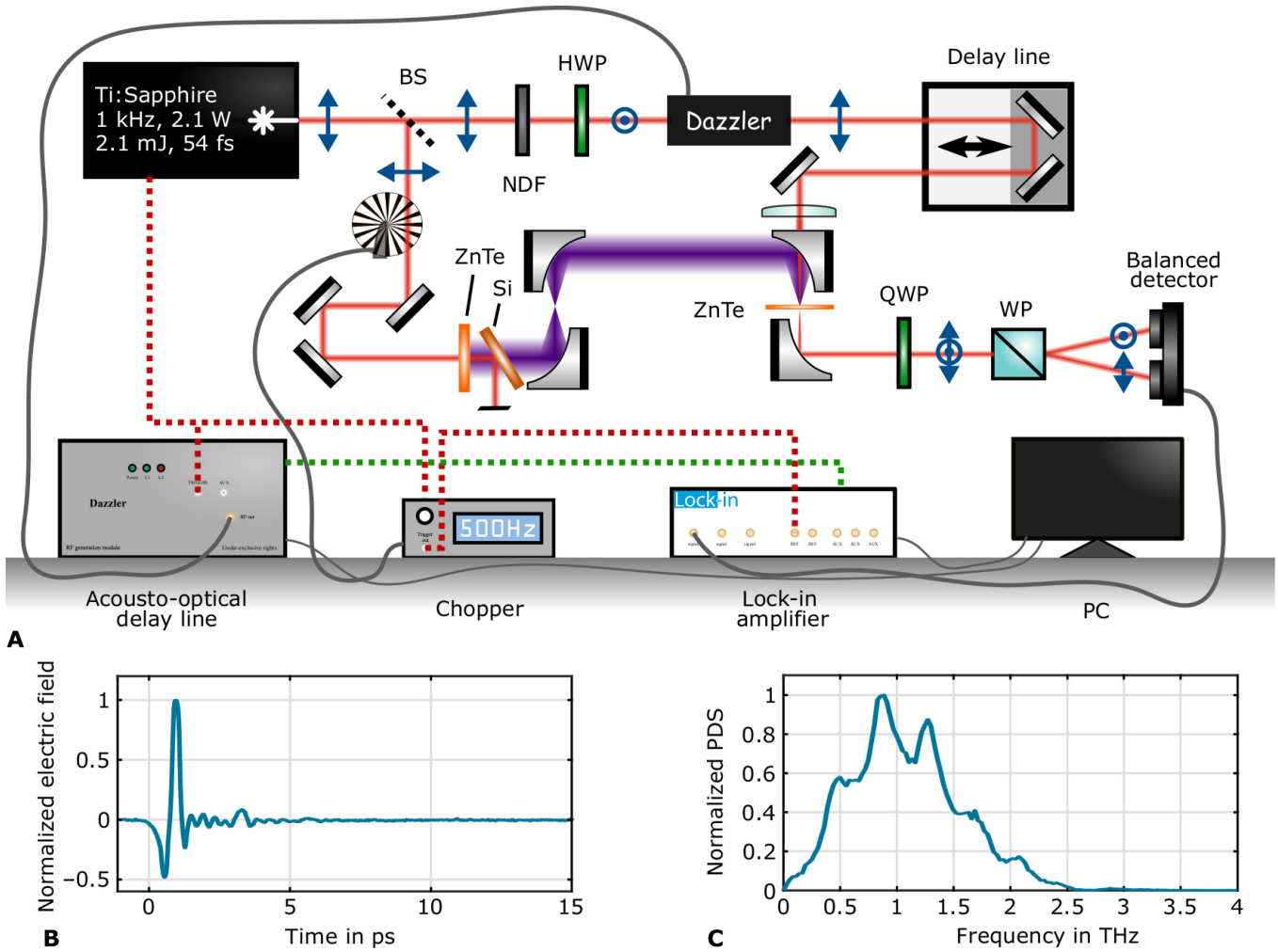

Fig. 2. (A) Details of the experimental setup. (B) Field-resolved measurement of the THz pulses via electro-optic sampling. (C) Spectrum of the THz pulses retrieved from the time-domain measurement. BS, beam splitter; HWP, half-wave plate; NDF, neutral density filter; QWP, quarter-wave plate; Si, silicon-plate; ZnTe, zinc telluride; WP, Wollaston prism.

from 4.1 to 2.8 mm at $1/e^2$ via a Gallilean beam expander with the focal length of $f = -100$ mm and $f = 150$ mm. The beam was then split into 2 paths via a 90:10 unpolarized beamsplitter. The reflected beam containing 90% of energy was chopped at a frequency of 500 Hz via a mechanical chopper. Therefore, every second pulse was blocked by the chopper. The modulated signal, in combination with a boxcar filter, was used to eliminate systematic drifts of the measurement. The modulated beam was used to generate THz transients via optical rectification in a 1-mm-thick ZnTe crystal (see Fig. 2B and C). After the THz generation, a 1.6-mm-thick silicon plate was used to filter the 800-nm pump beam while transmitting the THz-beam. The THz pulses propagated through a box filled and sealed with water vapor molecules at 50% relative humidity. Nitrogen was used to control the humidity of the sealed box.

An electro-optic sampling setup incorporating a 0.1-mm-thick ZnTe crystal was developed to characterize the electric field of the THz pulses. Forty microwatts of the amplifier's output power was used to probe the THz pulses at the electro-optic sampling stage, where the polarization changes of the probe pulse due to interaction with THz electric field strength was detected in an ellipsometer incorporating balanced photodiodes. The THz pulses were focused on the detection crystal with a pierced parabola with the focal length of $f = 50.3$ mm while spatially overlapped with the probe beam.

For real-time, random scanning of the probe pulses over the water vapor's molecular response, an acousto-optical delay line with kilohertz scanning rates was integrated into the probe's beam path [31,32]. The acousto-optic delay line allows for arbitrary relative time delay between the THz pulse and probe pulses and shot-to-shot random scanning of the electric field. In front of the Dazzler, the polarization of the probe was flipped via a half-waveplate to provide the required input polarization. The diffracted output beam from the Dazzler has an orthogonal polarization relative to the input beam. Eventually, the probe beam was focused through a pierced parabola to the detection crystal with a plano-convex lens ($f = 130$ mm). The THz-beam copropagated with the probe beam with altered polarization depending on the instantaneous THz field strength via the Pockels effect in the detection crystal. After collimation of the probe beam with an off-axis parabola ($f = 100$ mm), its polarization status was analyzed with an ellipsometric detection scheme consisting of a quarter-waveplate, a Wollaston prism, and a balanced photodetector. The signal of the balanced photodetector was fed into a lock-in amplifier using a boxcar filter to eliminate systematic drifts, while the lock-in amplifier's boxcar filter ensured the signal's high-bandwidth detection during the random scanning. Data acquisition was performed by the lock-in amplifier triggered by the radio frequency control signals from the acousto-optic delay line. Data acquisition trigger (green) and synchronization paths (red) are indicated in Fig. 2A by dashed lines. The time-delay module had a refresh time of 2 ms at an arbitrary temporal position within its scanning range. To capture the complete molecular response encoded in the THz field, which lasts for tens of picoseconds, a mechanical delay line was added to the acousto-optic delay line, extending the scanning range of 6,400 fs for a single acousto-optical delay line to >40 ps. Alternatively, the scanning range can be extended by coupling multiple acousto-optic modulators.

Reconstruction strategy

Two categories of compressed sensing algorithms [19,20] were investigated for reconstructing the electric field of water's randomly sampled molecular response: convex compressed sensing and greedy algorithm (see Fig. 3). Basis Pursuit Denoising (BPD) and Lasso algorithms [33,34] from the family of convex compressed sensing algorithms were used for reconstruction due to their noise robustness and low reconstruction error for signals with moderate sparsity [19,35]. When comparing the mean squared error of the reconstruction for both algorithms, it was noted that the Lasso algorithm has a unique global minimum at a specific threshold value in the optimization problem. In contrast, the BPD algorithm demonstrates a negligible mean squared error across a range of threshold parameters (τ and $\boldsymbol{\sigma}$ in supplementary information). BPD is also recognized for its ability to reduce the measurement noise of the oversampled signals [36]. As finding a reference for arbitrary measurements to optimize the reconstruction threshold value is not always

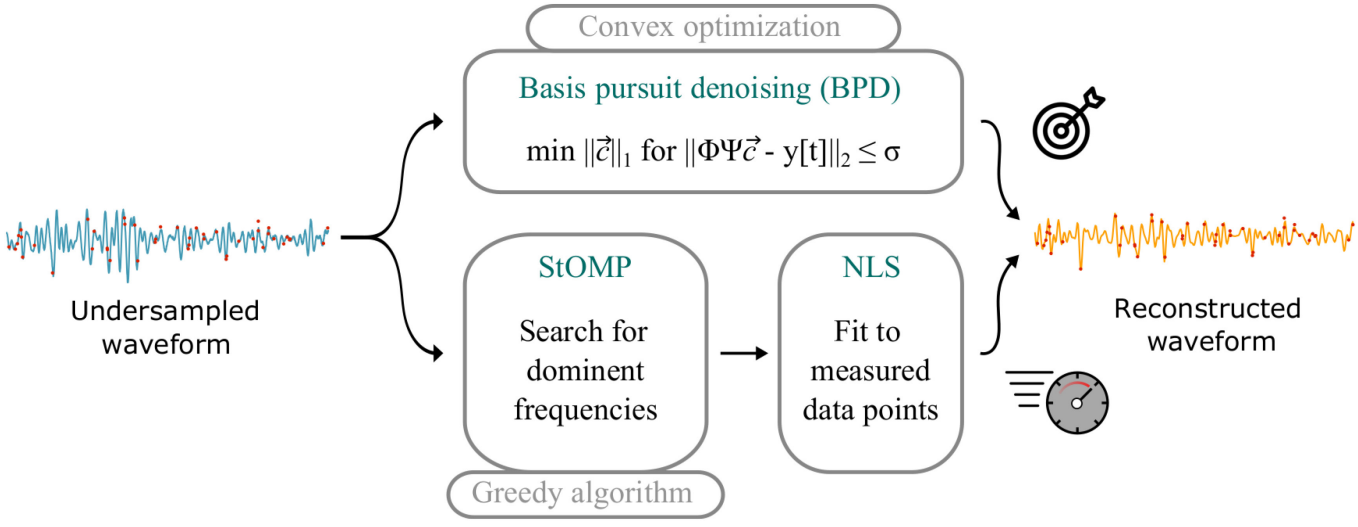

Fig. 3. The reconstruction algorithms used for the data analysis of the sparse measurements: The BPD and StOMP algorithms. While StOMP has the benefit of fast data processing, it requires an input reconstruction threshold value. To overcome this inefficiency, the IQR method was used to search for the dominant frequencies, while the Nonlinear Least Square algorithm was used to optimize the amplitude of the reconstructed traces.

feasible, BPD was selected for further analysis. From the second category, the Stagewise Orthogonal Matching Pursuit (StOMP) greedy algorithm was chosen and developed owing to its fast computation and robustness to noise [19]. To address the issue of significant amplitude reconstruction error in StOMP, a Nonlinear Least Square (NLS) algorithm has been incorporated into the StOMP reconstruction. Additionally, StOMP necessitates a distinct reconstruction threshold value at every iteration, which is inefficient and impractical. Consequently, an approach based on the interquartile range method [37] was developed to calculate the threshold parameter automatically (see supplementary information for more details).

Results

As a proof-of-principle experiment for time domain compressed sensing, we resolved atmospheric water vapor's spectroscopic information in response to the THz excitation pulses centered at 1 THz. Among the most abundant molecules in the atmosphere, only water possesses a permanent dipole in this spectral range [38]. As a result, the spectral coverage of THz excitation pulses serves as a filter, isolating the study to only water vapor and its isotopes [39]. The ambient air's absorption spectrum in this spectral range is characterized by a high density of absorption peaks [40], which makes it an ideal platform for assessing the efficacy of compressed sensing in reconstructing moderately sparse spectra while also highlighting its limitations in reconstructing prominent absorption peaks and adjunct frequencies. Moreover, such realization holds promise for real-time gas detection in open-air environments [41,42]. For a comparison between conventional sampling and compressed sensing, 2 categories of measurements with different numbers of sampling points were performed in real-time on the water vapor response: (a) linear scans with sampling points at the time intervals of $t_{n+1} = t_n + \Delta t$, and (b) uniformly random distributed sampling points. Each measurement was repeated 10 times. As a result, the location of the randomly located sample points of the second category varies for every measurement.

Ten oversampled, linearly scanned measurements of the molecular response with $N = 2{,}034$ sample points were averaged to generate a reference waveform. This reference trace is shown by the blue curve in Fig. 4A. The atmospheric vapor molecules are excited impulsively by the THz light transient, and their molecular response is temporarily separated from the broadband excitation pulse. This molecular response rich with spectroscopic information is sparse in the frequency domain as it only contains the information on resonance frequencies of the sample [43]. Therefore, the temporally gated signal from 5 to 35 ps was considered for compressed sensing. The upper limit of this range was determined by the internal reflection of the THz light transient at 36 ps. To evaluate the performance of the sparse sampling, the field-resolved molecular response was measured at 18 different sampling rates from 2,023 measured data points to 46 data points. The reconstruction was performed using both BPD and StOMP algorithms.

Figure 4A shows the real-time compressed sensing of the field-resolved molecular response of the atmospheric water. A single sparse measurement at an extreme limit with the minimum random number of sample points of $N = 46$, is shown by red dots. The orange and green curves show the reconstructed field using BPD and STOMP algorithms for $N = 46$, respectively. To evaluate the performance of compressed sensing, we calculated the mean squared error between the reference waveform and the reconstructed waveforms via BPD and StOMP, respectively.

Figure 4B shows the average and standard deviation of the mean squared error as a function of N for each algorithm. The

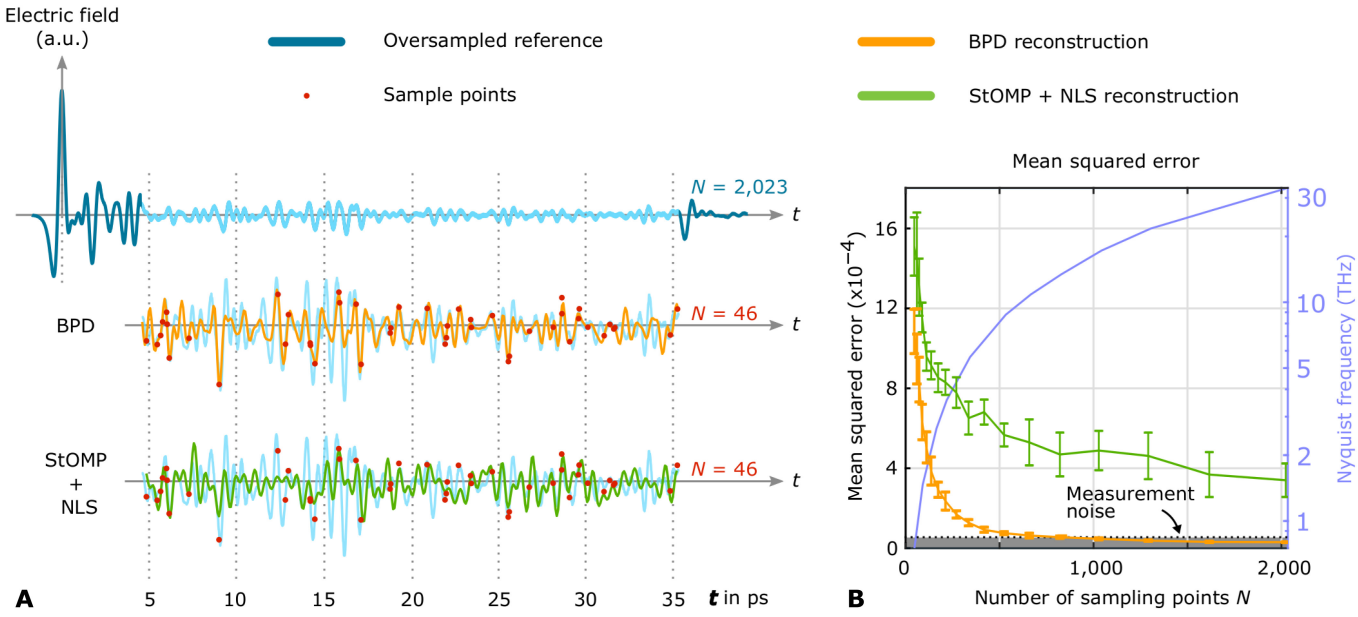

Fig. 4. (A) Real-time compressed sensing of the field-resolved molecular response of atmospheric water. The light blue curve shows the reference waveform, while the red dots illustrate the random sparse detection at $N = 46$ sampling points. The reconstructed waveform via the BPD and StOMP algorithms are shown in orange and green, respectively. (B) Mean Squared Error of the reconstructed waveforms via BPD and StOMP versus N. The purple curve shows the corresponding calculated Nyquist frequency for each N for comparison. The dotted line indicates the Mean Squared Error of linearly sampled measurements, indicating the measurement noise. By random sampling, the BDP filters and reduces noise from the oversampled signal. Therefore, the average of 10 reconstructed waveforms shows lower noise than the case of linearly sampled measurements.

purple curve shows the corresponding calculated Nyquist frequency for each N for comparison. The dotted line indicates the measurement noise. The measurement noise was calculated by averaging the mean squared error of the reference waveform versus the reconstructed waveform for each N. As this value exhibits only slight variations across different N, it is indicated by a horizontal dotted line. Not only does the BPD algorithm outperform the StOMP method, but for larger values of N, the waveforms reconstructed using BPD show a mean squared error lower than the measurement noise. This is due to the tendency of BPD to converge to a solution with maximum sparsity, which acts as a filter rejecting signal amplitudes other than absorption frequencies. For lower values of N, the mean squared error increases nonlinearly, reaching 12×10^{-4} at $N = 46$. The low standard deviation between the 10 different measurements for each value of N demonstrates the stability of the reconstructions.

Figure 5A displays the spectrum of the reference waveform and the sparse sampling measurements at various sampling points of $N = 524$, $N = 136$, and $N = 46$. These sampling data points correspond to Nyquist frequencies of 8.8, 2.3, and 0.8 THz, respectively. The spectra obtained from the compressed sensing reconstructed waveform successfully retrieve water absorption peaks beyond the Nyquist limit even for low sampling points of $N = 46$, which corresponds to temporal steps of $\Delta t = 666$ fs. The number of sampling points would need to be increased by at least 3 times to achieve a similar outcome using conventional sampling.

Figure 5B and C summarizes the performance of the BPD and StOMP reconstructions for measurements at various N, where the averaged Fourier transformation of the 10 compressed sensing reconstructed waveforms at different N are presented. The amplitude at each N is normalized to one, and the area bordered by the purple line denotes the recovered frequencies beyond the Nyquist limit. The spectral region ranging from 1 to 1.5 THz is crucial for this investigation due to several absorption lines with high cross-sections and the high spectral density of the THz excitation pulses. Remarkably, the primary absorption peaks in this region are exceptionally well recovered beyond the Nyquist limit with excellent quality. When dealing with lower values of N, the reconstruction of absorption lines with lower amplitude and adjunct frequencies is more noise-prone, even for those below the Nyquist limit. A comparison of Fig. 5D and Fig. 5E reveals that while the less complex StOMP algorithm has the potential of a fast reconstruction speed compared to BPD, it results in noisier reconstructions of both the low-amplitude frequencies below the Nyquist limit and the absorption lines beyond the Nyquist limit.

Conclusion

Ultrashort time-domain spectroscopy, particularly field-resolved spectroscopy, has been a gold standard for accurately identifying the constituents and dynamics of matter without the need for labels [14, 43–47]. Despite numerous attempts to increase measurement speed in ultrafast spectroscopy [32,48,49], real-time

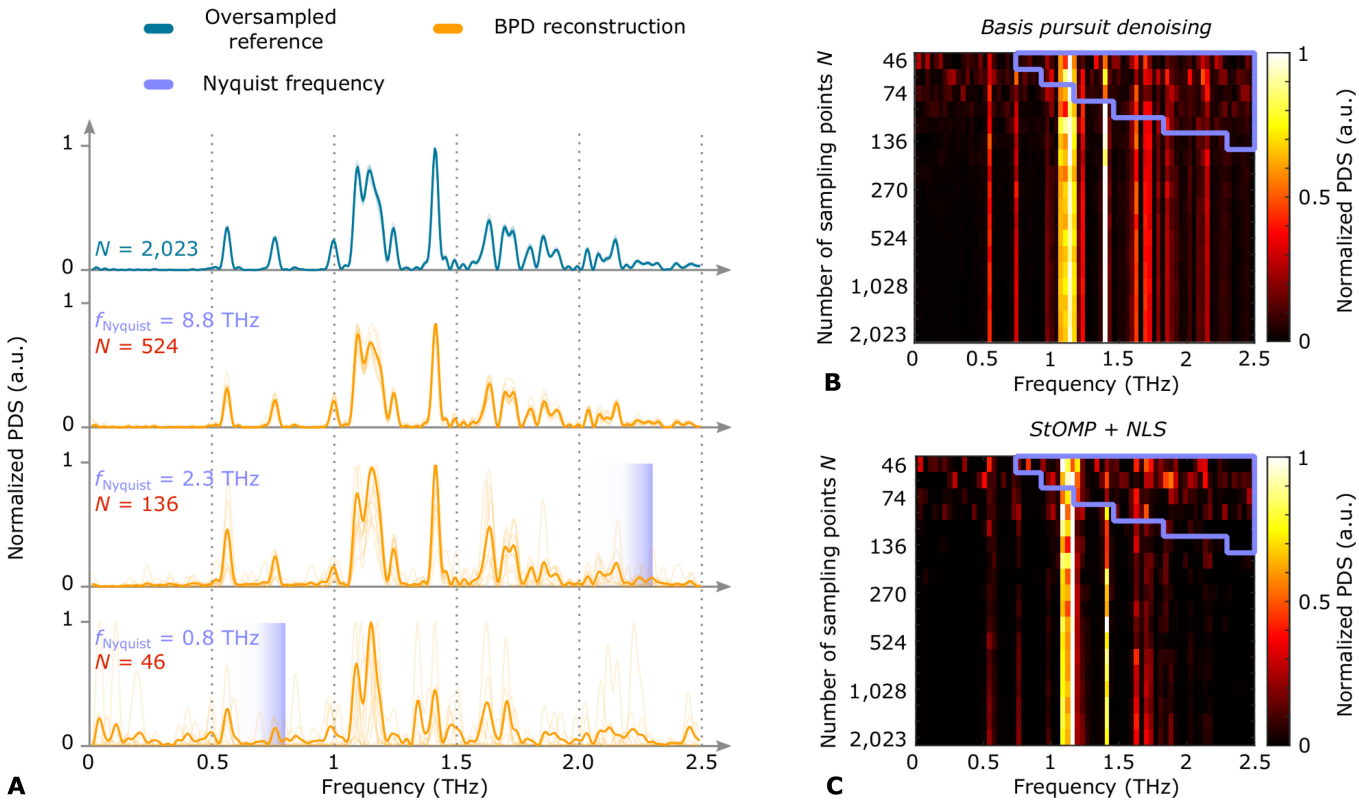

Fig. 5. (A) Fourier transform counterpart of the reference waveform and the sparse sampling measurements at various sampling points of $N = 524$, $N = 136$, and $N = 46$. The purple bars show the corresponding Nyquist frequency of each sampling data point. The transparent curve shows the variation in different random measurements. (B) Averaged reconstructed spectra by BPD at various N. (C) Averaged reconstructed spectra by StOMP at various N. The bordered purple area denotes the reconstructed spectral components beyond the Nyquist frequency.

measurements remain challenging due to a prolonged acquisition time, significant data volume, and processing time. This study showcases compressed sensing with rapidly sampled field-resolved spectroscopy for the first time, providing a solution to overcome these limitations. In particular, when short excitation laser pulses interact with matter, the signal-carrying information on this interaction is temporally separated from the main pulse, turning the characterization problem into a compressed sensing problem. Crucial for compressed sensing is the possibility of random sampling, which has been achieved by employing an acousto-optic delay line and a boxcar filter for broadband data acquisition with a high dynamic range. The relatively high density of absorption peaks of ambient air water in the THz spectral range provides an ideal platform for assessing the efficacy of compressed sensing in reconstructing moderately sparse spectra while highlighting its limitations. We report resolving the absorption frequencies 3 times higher than the Nyquist limit. By employing a cascaded acousto-optic delay line, the acquisition time of sparse sampling for $N = 46$ sampling points can be reduced to sub-100 ms. The acquisition time is at least 3 times higher for the linear sampling of the signal at a Nyquist frequency of 2.3 THz. Additionally, we demonstrate that compressed sensing below the Nyquist criteria can suppress measurement noise, making it valuable for speeding up measurement time and denoising sensitive measurements.

Determining when sufficient sample points have been acquired for measuring an unknown spectrum is a major challenge in compressed sensing. However, the uniform random sampling over the whole region of interest and real-time analysis of the measurement in less than 3 ms allows for the identification of the best-reconstructed waveform. As the refresh time of the acousto-optic delay line is at 30 kHz, individual random shot-to-shot sampling can be performed for laser pulses below this repetition rate. For higher repetition rates, partial random scanning can be performed. Here, each launched acoustic wave packet inside the acousto-optical delay line delays an incoming pulse train with equally spaced delays [32], while the relative delay between different scans is randomized, showing promise to introduce compressed sensing.

Real-time ultrafast spectroscopy is of crucial importance in various fields. Our innovative technique can greatly accelerate data acquisition in ultrafast spectroscopy, particularly in higher-dimensional analyses, by data volume minimization, signal acquisition time reduction, and a contraction in the required number of measurements in each dimension. These advances alleviate the requirements for specialized measurement instruments, offering benefits extending well beyond traditional spectroscopy applications. For instance, simplifying the handling of fragile specimens, enabling real-time environmental monitoring of short-lived pollutants, and real-time, open-air diagnostics of toxic and hazardous gases [15–17,50].

Acknowledgments

We thank P. J. Russell, F. Tani, M. Butryn, S. Malzer, and H. Potts for their support.

Funding: This work was supported by research funding from the Max Planck Society. K.S. is part of the Max Planck School of Photonics, supported by the German Federal Ministry of Education and Research (BMBF), the Max Planck Society, and the Fraunhofer Society.

Author contributions: H.F. envisioned the experiment. K.S. performed the measurements. H.J., S.C., N.F., K.S., and H.F. designed the random scanning. C.R. contributed to devising the strategy for data acquisition. K.S., J.W., and H.F. performed the data reconstruction and analysis. All authors reviewed and contributed to the manuscript text.

Competing interests: The authors declare no conflicts of interest.

Data Availability

The data may be obtained from the authors upon reasonable request.

Supplementary Materials

Sections S1 to S3
Figs. S1 to S6

References

1. Wang Z-G, Xia H-R. *Molecular and laser spectroscopy*, vol. 50. Heidelberg (Germany): Springer Science & Business Media; 2012.
2. Coutaz J-L, Garet F, Wallace V. *Principles of Terahertz time-domain spectroscopy*. Singapore (Republic of Singapore): CRC Press; 2018.
3. Zewail AH. Femtochemistry: Atomic-scale dynamics of the chemical bond†. *Chem Eur J*. 2000;104:5660–5694.
4. Keilmann F, Gohle C, Holzwarth R. Time-domain mid-infrared frequency-comb spectrometer. *Opt Lett*. 2004;29(13):1542–1544.
5. Schiller S. Spectrometry with frequency combs. *Opt Lett*. 2002;27:766–768.
6. Picqué N, Hänsch TW. Frequency comb spectroscopy. *Nat Photonics*. 2019;13:146–157.
7. Lanin AA, Voronin AA, Fedotov AB, Zheltikov AM. Time-domain spectroscopy in the mid-infrared. *Sci Rep*. 2014;4:6670.
8. Wu Q, Zhang X. Free-space electro-optic sampling of terahertz beams. *Appl Phys Lett*. 1995;67(24):3523–3525.
9. Timmers H, Kowligy A, Lind A, Cruz FC, Nader N, Silfies M, Ycas G, Allison TK, Schunemann PG, Papp SB. Molecular fingerprinting with bright, broadband infrared frequency combs. *Optica*. 2018;5(6):727–732.
10. Laubereau A, Kaiser W. Vibrational dynamics of liquids and solids investigated by picosecond light pulses. *Rev Mod Phys*. 1978;50:607–665.
11. Movasaghi Z, Rehman S. Fourier transform infrared (FTIR) spectroscopy of biological tissues. *Appl Spectrosc Rev*. 2008;43(2):134–179.
12. Pupeza I, Huber M, Trubetskov M, Schweinberger W, Hussain SA, Hofer C, Fritsch K, Poetzlberger M, Vamos L, Fill E, et al. Field-resolved infrared spectroscopy of biological systems. *Nature*. 2020;577:52–59.
13. Kowligy AS, Timmers H, Lind AJ, Elu U, Cruz FC, Schunemann PG, Biegert J, Diddams SA. Infrared electric field sampled frequency comb spectroscopy. *Sci Adv*. 2019;5(6):Article eaaw8794.
14. Herbst A, Scheffter K, Bidhendi MM, Kieker M, Srivastava A, Fattahi H. Recent advances in petahertz electric field sampling. *J Phys B: At Mol Optical Phys*. 2022;55(17):Article 172001.
15. Smallwood CL, Cundiff ST, et al. *Laser Photonics Rev*. 2018;12(12):Article 1800171.
16. Cocker TL, Peller D, Yu P, Repp J, Huber R. Tracking the ultrafast motion of a single molecule by femtosecond orbital imaging. *Nature*. 2016;539(7628):263–267.

17. Vicentini E, Wang Z, Van Gasse K, Hänsch TW, Picqué N. Dual-comb hyperspectral digital holography. *Nat Photonics*. 2021;15:890–894.
18. Edgar MP, Gibson GM, Padgett MJ. Principles and prospects for single-pixel imaging. *Nat Photonics*. 2019;13(1):13–20.
19. Rani M, Dhok SB, Deshmukh RB. A systematic review of compressive sensing: Concepts, implementations and applications. *IEEE Access*. 2018;6:4875–4894.
20. Candes EJ, Wakin MB. An introduction to compressive sampling. *IEEE Signal Process Mag*. 2008;25(2):21–30.
21. Candes E, Romberg J, Tao T. Robust uncertainty principles: Exact signal reconstruction from highly incomplete frequency information. *IEEE Trans Inf Theory*. 2006;52(2):489–509.
22. Donoho D. Compressed sensing. *IEEE Trans Inf Theory*. 2006;52(4):1289–1306.
23. Candes EJ, Tao T. Near-optimal signal recovery from random projections: Universal encoding strategies? *IEEE Trans Inf Theory*. 2006;52(12):5406–5425.
24. Ostic R, Ménard J-M. Speeding up ultrafast spectroscopy. *Physics*. 2021;14:23.
25. Takizawa S, Hiramatsu K, Goda K. Compressed time-domain coherent raman spectroscopy with real-time random sampling. *Vib Spectrosc*. 2020;107:103042.
26. Adhikari S, Cortes CL, Wen X, Panuganti S, Gosztola DJ, Schaller RD, Wiederrecht GP, Gray SK. Accelerating ultrafast spectroscopy with compressive sensing. *Phys Rev Appl*. 2021;15:Article 024032.
27. Katz O, Levitt J, Silberberg Y, Compressive fourier transform spectroscopy. arXiv. 2010. https://doi.org/10.48550/arXiv.1006.2553
28. Kaestner B, Schmähling F, Hornemann A, Ulrich G, Hoehl A, Kruskopf M, Pierz K, Raschke M, Wübbeler G, Elster C. Compressed sensing ftir nano-spectroscopy and nano-imaging. *Opt Express*. 2018;26(14):18115–18115.
29. Kawai A, Kageyama T, Horisaki R, Ideguchi T. Compressive dual-comb spectroscopy. *Sci Rep*. 2021;11(1):13494.
30. Zhu N, Xu Z, Wang Z, Song Z, Wang W, Chen X, Chao X. Midinfrared compressed fourier-transform spectroscopy with an optical frequency comb. *Phys Rev Appl*. 2022;18:Article 024025.
31. Kaplan D, Tournois P. Theory and performance of the acousto optic programmable dispersive filter used for femtosecond laser pulse shaping. *J Phys IV France*. 2002;12(5):69–75.
32. Schubert O, Eisele M, Crozatier V, Forget N, Kaplan D, Huber R. Rapid-scan acousto-optical delay line with 34 khz scan rate and 15 as precision. *Opt Lett*. 2013;38(15):2907–2910.
33. van den Berg E, Friedlander MP. Probing the pareto frontier for basis pursuit solutions. *SIAM J Sci Comput*. 2008;31(2):890–912.
34. van den Berg E, Friedlander MP. SPGL1: A solver for large-scale sparse reconstruction, December 2019. https://friedlander.io/spgl1.
35. Arjoune Y, Kaabouch N, El Ghazi H, Tamtaoui A. Compressive sensing: Performance comparison of sparse recovery algorithms. Paper presented at: 2017 IEEE 7th Annual Computing and Communication Workshop and Conference (CCWC); 2017 Jan 09–11; Las Vegas, NV.
36. Chen SS, Donoho DL, Saunders MA. Atomic decomposition by basis pursuit. *SIAM Rev*. 2001;43(1):129–159.
37. Dekking FM, Kraaikamp C, Lopuhaä HP, Meester LE, *A Modern introduction to probability and statistics: Understanding why and how*, vol. 488. London (UK): Springer; 2005.
38. Cox AN. *Allen's astrophysical quantities*. New York (NY): Springer; 2015.
39. van Exter M, Fattinger C, Grischkowsky D. Terahertz time-domain spectroscopy of water vapor. *Opt Lett*. 1989;14:1128–1130.
40. Cui H, Zhang X, Su J, Yang Y, Fang Q, Wei X. Vibration-rotation absorption spectrum of water vapor molecular in frequency selector at 0.5-2.5thz range. *Optik*. 2015;126(23):3533–3537.
41. Sitnikov DS, Romashevskiy SA, Pronkin AA, Ilina IV. Open-path gas detection using terahertz time-domain spectroscopy. *J Phys Conf Ser*. 2019:1147, Article 012061.
42. Liu H-B, Zhong H, Karpowicz N, Chen Y, Zhang X-C. Terahertz spectroscopy and imaging for defense and security applications. *Proc IEEE*. 2007;95(8):1514–1527.
43. A. Srivastava, A. Herbst, M. M. Bidhendi, M. Kieker, F. Tani, and H. Fattahi. Near-petahertz fieldoscopy of liquid. arXiv. 2023. https://doi.org/10.48550/arXiv.1006.2553
44. Riek C, Seletskiy DV, Moskalenko AS, Schmidt J, Krauspe P, Eckart S, Eggert S, Burkard G, Leitenstorfer A. Direct sampling of electric-field vacuum fluctuations. *Science*. 2015;350(6259):420–423.
45. Krausz F, Ivanov M. Attosecond physics. *Rev Mod Phys*. 2009;81:163–234.
46. Pandey S, Tan LZ, Walz F, Makhija V, Shivaram N. Ultrafast field-resolved nonlinear optical spectroscopy in the molecular frame. arXiv. 2023. https://doi.org/10.48550/arXiv.2311.18230
47. Fattahi H. Sub-cycle light transients for attosecond, x-ray, four-dimensional imaging. *Contemp Phys*. 2016;57(4):580–595.
48. Weigel A, Jacob P, Gröters D, Buberl T, Huber M, Trubetskov M, Heberle J, Pupeza I. Ultra-rapid electro-optic sampling of octave-spanning mid-infrared waveforms. *Opt Express*. 2021;29(13):20747–20764.
49. Mohler KJ, Bohn BJ, Yan M, Mélen G, Hänsch TW, Picqué N. Dual-comb coherent raman spectroscopy with lasers of 1-ghz pulse repetition frequency. *Opt Lett*. 2017;42(2):318–321.
50. Jun S, Herbst A, Scheffter K, John N, Kolb J, Wehner D, Fattahi H, Highly nonlinear dynamics of deep tissue upon in vivo interaction with femtosecond laser pulses at 1030 nm. arXiv. 2023. https://doi.org/10.48550/arXiv.2308.05453